Reversible microfluidics device for precious metal electrodeposition and depletion yield studies

Jérémie Gouyon, Fanny d'Orlyé, Craig Simon, Sophie Griveau, Catherine Sella, Laurent Thouin, Féthi Bedioui, Anne Varenne

To cite this version:

Jérémie Gouyon, Fanny d'Orlyé, Craig Simon, Sophie Griveau, Catherine Sella, et al.. Reversible microfluidics device for precious metal electrodeposition and depletion yield studies. Electrochimica Acta, 2020, 352, pp.136474. 10.1016/j.electacta.2020.136474 . hal-03919332

HAL Id: hal-03919332
https://hal.science/hal-03919332

Submitted on 21 May 2024

Reversible microfluidics device for precious metal electrodeposition and depletion yield studies

Jérémie Gouyon [1,2], Fanny d'Orlyé [1], Craig Simon [1,3], Sophie Griveau [1], Catherine Sella [4], Laurent Thouin [4], Fethi Bedioui [1], Anne Varenne [1*]

[1] Chimie ParisTech, PSL University, CNRS 2027, Institute of Chemistry for Life and Health Sciences, SEISAD 75005 Paris, France.

[2] French Environment and Energy Management Agency, 20, avenue du Grésillé- BP 90406 49004 Angers Cedex 01, France

[3] University of Strathclyde, Glasgow G1 1XQ, United Kingdom

[4] PASTEUR, Département de chimie, École normale supérieure, PSL Université, Sorbonne Université, CNRS, 75005 Paris, France

E-mail: anne.varenne@chimieparistech.psl.eu (Varenne A.)

Abstract

A new low-cost reversible Glass-NOA®-PDMS microfluidic device was designed for the study of recovery yield of precious metals present in acid media mimicking leach liquors for long-term recycling objectives. It offers the unique advantage of allowing easy washing of the microchannel and renewal of the electrode surface by simply repositioning the microband electrodes which allows this type of device to have a relatively much longer lifespan than irreversibly closed ones. It consists in a re-usable microchip with four graphite microbands electrodes, prepared by screen printing, to set-up an original amperometric device for both depletion and yield quantification. One upstream working electrode is devoted to the depletion of the metallic ions through their electrolysis by electrodeposition while the second downstream working microelectrode is used as real-time detection electrode to evaluate the depletion efficiency. The dimensions of the depletion electrode and of the channel were optimized thanks to numerical simulations for a given range of flow velocities. First, the performances of the device were assessed experimentally according to flow rate and applied potential under continuous flow, and then compared to theoretical predictions using an electrochemical probe, ferrocenemethanol. The proof of concept was then demonstrated for precious metal, by electroreduction of Pd(II) and Au(III) from acidic leach liquors under continuous flow, with a depletion yield of up to 89% and 71% respectively.

Keywords

Precious metals – Microfluidic – Depletion – Electrodeposition

1. Introduction

Printed circuit boards (PCBs) are known as an integral part of our technological devices (smartphones, computers…). As their use has become more and more important in the recent decades, the amount of waste is increasing and becomes an ecological, economic and strategic challenge [1,2]. Indeed, waste PCBs are a major source of strategic metals [3], such as platinum group metals (PGM), rare earth elements or other expensive species. Their recovery is crucial, especially since some of them are defined as critical (supply risks, high cost) by the European Commission [4] since 2014, such as Platinum (Pt) or Palladium (Pd). Their recycling is generally carried out in a three steps process [5]: (i) a mechanical grinding to reduce PCBs to powders and separate ferrous and non-ferrous metals, (ii) pyrolysis at 1000°C to remove the organic constituents and (iii) a hydrometallurgical treatment to selectively remove metals in ionic form in leaching solutions. These treatments are thus promising in terms of strategic metals recovery rate, but purification methods are still time-consuming and need to be optimized to ensure high purity of recycled materials, especially in their metallic form.

Thanks to microfluidics [6], the change in scale from an industrial process to microchannel results in a modification of the mechanical properties of fluids. This allows leading to high conversion for organic synthesis, for example, and high purity of the products [7,8]. In addition, the low manufacturing cost of microreactors permits them to be parallelized, allowing for processing a large quantity of samples, thus competing with current industrial macro-processes [9]. Even if diagnosis is one of the main application of microfluidics (for environmental [10] and biological [11] survey), the use of such miniaturized tools for the treatment of large amounts of liquid is also feasible.

Microfluidic coupled to the integration of electrodes within microchannels has been previously used to remove potential interfering agents from real samples but also to increase the selectivity towards a target (such as oxalic acid or nitric oxide) during its electrochemical detection [12,13]. The developed setups are composed of a four-electrodes cell, where two working electrodes (WE) are placed perpendicularly to a single microchannel containing the solution under continuous flow. Watanabe et al. [12] used a large WE (WE_{DEP}, depletion electrode) in order to remove the electroactive analyte (ferricyanide) from the solution and checked the depletion yield by measuring ferricyanide concentration thanks to the second WE (WE_{det}, detection electrode) positioned downstream. The importance of main parameters on the depletion yield has been discussed by the authors such as ratio of electrode width to channel height, flow velocity and applied potentials. The authors stated that their setup was not suitable to complete the depletion up to 100 % due to the height of the channel which was larger than the convection-diffusion layer of the sample. Indeed, the thin-layer regime at the electrode must be achieved under mass transport control for complete depletion [14–16]. More recently, similar strategy was adopted for the assessment of global antioxidant capacity and for the depletion of hydrogen peroxide (up to

95%) [13]. In this last case, the selectivity of nitric oxide detection was enhanced by positioning a NO-sensor downstream of the depletion electrode. It should be noted that the devices described in the literature for this type of application are sealed and do not offer any possibility of easy and quick reuse in case of pollution of the depletion electrodes and their regeneration.

Reversibly bonded chips reported in the literature are generally used for other applications such as coupling of electrophoresis with electrochemical detection or surface patterning for bio-molecule analysis [17]. Several strategies for the reversible bonding of the different parts of the microdevices were used such as magnetism, vaccum or spontaneous conformal contact between PDMS and glass [18] or other materials (metals, acrylate plate [19]). They offer the main advantage of facilitating the washing and the renewability of channels. We propose in this study an original microfluidic device to address the issue of recovering Au and Pd dissolved in acidic media (as $AuCl_4^-$ and $PdCl_4^{2-}$ respectively), mimicking leach liquors from the waste PCBs recycling process. For this purpose, a re-usable new reversible Glass-NOA®-PDMS microchip with four graphite microbands electrodes adapted from previously developed one by our group [20], was designed to set-up an original amperometric recovery device for both depletion and yield quantification. The device reported here offers the unique advantage of being a micro sandwich system with a reversible bond composed of two parts without the need for a magnetic or other device to maintain perfect adhesion, allowing easy washing of the microchannel and renewal of the electrode surface by simply repositioning the microband electrodes. This configuration permits enhancing its lifetime. First, to optimize the performance of the proposed microdevice, ferrocene methanol was used as a model. Then, the method efficiency for precious metallic species were discussed and compared to theoretical predictions.

2. Materials and methods

2.1. Chemicals

Standard solution of Gold Standard for ICP TraceCERT® 1000 mg/L (5% HCl) and Palladium Standard for ICP TraceCERT® 10000 mg/L (10% HCl with HNO_3^- traces), ferrocene methanol (noted as FcMeOH, 97%), sodium phosphate dibasic (99%), sodium phosphate monobasic (99%) were purchased from Sigma-Aldrich (Germany). HCl (37%) was purchased from Acros Organics (France). Graphite powder (2-15µm microcrystal grade 99.9995%) was obtained from Alfa Aesar (Germany), PDMS RTV 615 kit was obtained from Mentiv (France), PDMS Sylgard 184 kit from Dow Corning (Germany), SU8 2075 from Microchem (USA), and Norland Optical Adhesive 81® (noted as NOA81®) from Epotecny (France) and were used for fabrication of microchannels and microelectrodes. Ultrapure water was obtained from a Purelab Flex System (18.2 MΩ.cm Veolia, France).

2.2. Solutions

The artificial leach liquors were prepared by dilution of appropriate amounts of metallic standard solutions with HCl in ultrapure water so as to obtain a 0.1 mol L^{-1} HCl solution. 200 µmol L^{-1} FcMeOH was prepared in 0.2 mol L^{-1} phosphate buffer (pH 6.7) with sonication for at least 2 hours to complete solubilization.

2.3. Microelectrode and microchip fabrication

The microfabrication process, developed in our lab, has been previously described [20]. Briefly, for the electrode fabrication, PDMS substrates containing microchannels of desired width are prepared by soft-lithography technic. A pattern is molded by UV exposure of spin-coated SU-8 on a silicon wafer with a photomask containing the design of the electrodes. Electrode pattern were printed on Kimolek® Paper with a Filmstar® photoplotter (Bernier Electronik, France). PDMS is spread on the surface of the mold prior to degassing and reticulating at 70°C for 1h. A mix of graphite powder and PDMS (C-PDMS, 1:1, w/w) is spread in the microchannels and polished by hand to remove the excess. The resulting electrodes are placed in an oven at 70°C for 3h before use. For the microchannel fabrication, a PDMS mold containing the positive pattern is prepared by the same technic. The mold is applied on top of a glass substrate previously covered with NOA$^{®}$81. After UV exposure, the open-channel is revealed by properly demolding the PDMS mold. The two parts are then assembled so as to close the chip, forming a spontaneous conformal contact between the open-channel (NOA81$^{®}$) and the electrode (C-PDMS on PDMS substrate). The scheme and a picture of the setup are shown in Figure 1. In such a device, WE_{DEP} is the working electrode dedicated to the depletion process (and also to the recovery of the metals), WE_{det} is the working electrode dedicated to the determination of the considered species and thus to the evaluation of the recovery efficiency.

Figure 1 – (a) Scheme of microchannel with four integrated C/PDMS microbands electrodes. WE_{DEP} is dedicated to the depletion process (and thus to the recovery), WE_{det} is dedicated to the determination of the considered species and thus to the evaluation of the recovery efficiency. Dimensions in µm (unless specified). * upper part of the setup (NOA81$^{®}$ microchannel; ** lower part of the setup (C-PDMS electrodes in PDMS substrate) (b) Photography of the experimental setup

2.4. Electrochemical measurement and depletion

Chronoamperometric (CA) and cyclic voltammetric (CV) measurements were performed with an Autolab PGSTAT 128N potentiostat (Metrohm), in a four electrodes cell (two WE coupled to one reference electrode RE and one counter electrode CE). The CVs were performed at 25 mV s^{-1} for each electrode to determine the potential required for CA, with RE connected to the 100 µm strip electrode and the CE connected to the 1000 µm strip electrode. The WE dedicated to the depletion (WE_{DEP}) was located upstream (500 µm width) along the flow direction, and the one dedicated to detection for control (WE_{det}) was positioned downstream (50 µm width). The flow of the solution along the microchannel was insured by a flow controller (MFCS^{TM}-EZ and flow rate sensor S, Fluigent, France), applying a negative pressure (0 to -345 mbar) from the outlet of the channel to prevent detachment of the reversibly sealed chip. The depletion yield for FcMeOH, Pd and Au were estimated by measuring in CA the difference in oxidation charge generated on the WE_{det} with and without polarization of WE_{DEP}, after substraction of charges measured with a blank sample (phosphate buffer or HCl alone). The depletion yield for FcMeOH was also evaluated from steady-state currents in CV.

The dimensions of the channels and of the electrode as well as the estimation of the depletion yield were first optimized by performing numerical simulations using COMSOL Multiphysics 5.3, through a similar approach as previously described [13]. Briefly, a laminar flow was considered in a rectangular microchannel by assuming a parabolic velocity profile in a two-dimension. The electrochemical reactions were supposed to be limited by mass transport and the diffusion-convection equation was solved numerically by finite elements. As a boundary condition, concentration of the analyte was imposed to 0 mol L^{-1} at the polarized electrode surface. The diffusion coefficient of the analyte was assumed equal to $7.6.10^{-6}$ cm^2 s^{-1}, which is the one of FcMeOH used as a model [21]. Simulations provided an optimal size of WE_{DEP} versus the channel height, within the range of flow velocities that could be used experimentally. According to the configuration and geometry of the microdevice described in Figure 1, depletion yields up to 95 % were expected for flow rate lower than 2 µL min^{-1}. The device was then applied to the recovery of Pd(II) and Au(III).

3. Results and discussion

3.1. Electrochemical behavior of FcMeOH under continuous flow

The electrochemical behavior of FcMeOH has been studied in the present configuration by CV on both WEs without flow (static mode) and under continuous flow (from 1 to 5 µL min^{-1}), as shown on Figure 2. The oxidation current for both WEs (WE$_{DEP}$ and WE$_{det}$) increase with the flow rate due to convection induced by continuous flow, leading to a steady-state mass transport to the electrodes and the observation of limiting currents. As expected in convective regimes, limiting currents increase linearly with the cubic root of flow rate (see inserts). At the highest flow rate (5 µL min^{-1}, *i.e.* 2.1 mm s^{-1}), the faradic current started from about 0.1V and reached a limiting value only for potential values higher than 0.5V due mainly to ohmic drop. According to these voltammograms the potential on both electrodes should be comprised between +0.5 and +1.0 V to ensure a constant oxidation current under continuous flow (for 1 to 5 µL min^{-1}) for optimal operating conditions. Indeed, to guarantee an optimum depletion efficiency (see sections below), the process needs to be performed at potential values that do not lead to a drastic current variation.

Figure 2 – Cyclic voltammograms of 200 µmol L^{-1} FcMeOH in 0.2 mol L^{-1} phosphate buffer at (a) WE$_{DEP}$ and (b) WE$_{det}$, in static mode (full line) and under continuous flow (from 1 to 5 µL min^{-1}). Scan rate: 25 mV s^{-1}. Inserts correspond to the plots of limiting currents as a function of cubic root of flow rate.

3.2. FcMeOH depletion

Cyclic voltammograms (CV) were performed at WE$_{det}$ with and without polarization of WE$_{DEP}$ at a constant potential of +1.0 V. Figure 3-a shows the mean values of limiting currents, noted as $I_{lim,WEdet}$, monitored under these conditions at WE$_{det}$ as a function of flow rate. The depletion yield (Figure 3-b) was determined from these data by calculating the ratio between limiting currents at WE$_{\mathrm{det}}$ (corrected from residual currents) with and without polarization of WE$_{\mathrm{DEP}}$:

$$Depletion\ yield_{CV}\ (\%) = \left(1 - \frac{I_{lim,WEdet}\ with\ WE_{DEP}^{ON}}{I_{lim,WEdet}\ with\ WE_{DEP}^{OFF}}\right) \times 100 \qquad \textbf{\textit{eq.1}}$$

As expected theoretically, the depletion yield decreases by increasing the flow rate: the higher the flow, the shorter the residence time of redox species near the depletion electrode. However, experimental depletion yields were lower (by a factor ranging between 1.2 to 2) than the ones predicted by simulation, as shown in Figure 3-b.

Figure 3 – (a) Limiting currents measured by cyclic voltammetry (from data in Fig. 2) at WE$_{\mathrm{det}}$ without (OFF) and with (ON) polarization of WE$_{\mathrm{DEP}}$. (b) Corresponding depletion yield evaluated from eq.1 as a function of flow rate. WE$_{\mathrm{DEP}}$ is biased at 1.0 V when polarized (ON).

The depletion process was also evaluated by chronoamperometry (CA). More precisely, consecutive potential steps (ON) and (OFF) were performed at WE$_{\mathrm{DEP}}$, while maintaining WE$_{\mathrm{det}}$ at a constant potential of 1 V for oxidizing remaining FcMeOH (Figure 4). Note that polarization of WE$_{\mathrm{DEP}}$, at 1 V and 0 V corresponds to the activation (ON) and deactivation (OFF) of the depletion process, respectively. As expected, polarization of WE$_{\mathrm{DEP}}$ at +1,0V leads *(i)* to the increase of currents characteristic of FcMeOH oxidation and *(ii)* to a decrease of currents at WE$_{\mathrm{det}}$ due to FcMeOH depletion. With this configuration of device and electrode material, the time delay to reach steady-state currents was estimated about 10 s.

Figure 4 – (a) Potential steps applied to WE$_{\mathrm{DEP}}$ for successive activations (1 V) and deactivations (0 V) of the depletion process. WE$_{\mathrm{det}}$ is continuously polarized at 1 V. (b) Corresponding chronoamperograms monitored at WE$_{\mathrm{det}}$ (full line) and WE$_{\mathrm{DEP}}$ (dashed line). 200 µmol L^{-1} FcMeOH in 0.2 mol L^{-1} phosphate buffer and flow rate of 1 µL min^{-1}.

Then, similar experiments were conducted on a longer time scale. Figure 5-a shows chronoamperograms obtained at WE$_{\mathrm{det}}$ for low flow rate (1 µL min^{-1} , *i.e.* 0.4 mm s^{-1}) with or without polarization of WE_{DEP}. First, a potential of 0 V was applied to WE_{det} during 30 s for stabilization of the baseline followed by a potential step to 1.0 V during 60 s. This procedure was applied either in presence of FcMeOH or in PBS to consider the influence of residual currents into the evaluation of the charges developed at WE_{det}, noted as Q_{WEdet}. Experiments were also carried out for other flow rates. Thus Figure 5-b shows the evolution of Q_{WEdet} during the second step as a function of flow rate, with or without polarization of WE_{DEP}. These data allowed evaluating in Figure 5-c the corresponding depletion yields (with subtraction of charge measured in PBS) according to the equation

$$Depletion\ yield_{CA}\ (\%) = \left(1 - \frac{Q_{WEdet}\ with\ WE_{DEP}^{ON}}{Q_{WEdet}\ with\ WE_{DEP}^{OFF}}\right) \times 100 \qquad \textbf{\textit{eq.2}}$$

Figure 5 – (a) Chronoamperometry at WE_{det} (30 s at 0 V and 60 s at 1.0 V) without depletion (curves 1 and 2, WE_{DEP} OFF) and with depletion (curves 3 and 4, WE_{DEP} polarized at 1 V) at 1 µL min^{-1} flow rate. (b) Experimental charge Q_{WEdet} developed at WE_{det} during the second step as a function of flow rate. (c) Depletion yield evaluated by eq. 2 from experimental data (cross points, dashed line) and simulations (solid curve) as a function of flow rate (200 µmol L^{-1} FcMeOH in 0.2 mol L^{-1} phosphate buffer).

In comparison to data obtained by CV (Figure 3-b) the same behavior was observed as a function of flow rate. A maximal depletion yield of 76.4% at the lowest flow rate 1 µL min^{-1}. The discrepancy between experimental and simulated data was similar. Indeed, the experimental depletion yields were lower than the predicted ones with: 76.4±3.3 % versus 99.6 at 1 µL min^{-1} and 41.1±7.0 % versus 73.4 % at 4 µL min^{-1}. As for data obtained by CV, this can be attributed to the composite material C-PDMS of the electrodes that does not lead to a well-defined active surface, perfectly planar, homogeneous, with no cavity or deformation. As shown by SEM [20], the C-PDMS electrodes cannot be considered as planar for simulations. Also, the ohmic drop can reduce the performances of the depletion process if steady-state current at WE_{DEP}, related to mass-transport limitation, is not reached at the applied potential. The larger the WE_{DEP}; the higher the influence of ohmic drop on depletion yield. However, according to our previous experiments, the potential of 1.0 V that was applied at both electrodes was sufficiently high to overcome the ohmic drop and to implement a process fully limited by mass transport. Therefore, only surface defaults and inactive areas of the C-PDMS electrodes could explain the deviations observed from numerical simulations.

Compared to the previously mentioned literature [13], performance of this microdevice is lower. In our case, the electrode material and aspect lead to significant differences since simulation did not consider the exact shape and nature of the material, and thus cannot reach the same level of efficiency than other metal electrode material. But since this system is of low fabrication cost, C-PDMS electrode material is of interest to counteract the onerous and technically laborious development of platinum electrodes. Also the eventual electrode passivation after successive runs and its potential pollution are overcompensated by the originality of this reversible system. Indeed, in case of major pollution of the electrodes during depletion processes, the device can be re-used as many times as portions of the band electrodes have not been exposed to the electrolyte solution. This is clearly an advantage compared to previously developed irreversibly closed depletion systems. In the case of FcMeOH study, no passivation was observed for the duration of the study on the different electrode areas used as continuous monitoring of blank samples was performed between each analysis so as to check the electrode and eventually renew the electroactive surface to avoid potential deterioration of the system.

3.4. Electrochemical reduction of chlorocomplexes of gold and palladium

The electrochemical activity of the different metal complexes has been previously examined on glassy carbon electrode in HCl solution [22,23], with electrodeposition occurring for potential value of 0 V for Pd and 0.35 V for Au. Pd and Au in HCl solution can be reduced and metals can be deposited according to the following reactions:

$$[PdCl_4^{2-}] + 2e \rightarrow Pd + 4Cl^- \qquad \textbf{\textit{(eq.3)}}$$

$$\begin{gathered} [AuCl_4^-] + 2e \rightarrow [AuCl_2^-] + 2Cl^- \\ 3[AuCl_2^-] \rightarrow 2Au + [AuCl_4^-] + 2Cl^- \end{gathered} \qquad \textbf{\textit{(eq.4)}}$$

Their electrodeposition on C-PDMS microelectrode within a microchannel occurs similarly but at different potentials (about -0.3 V and -0.5 V/C-PDMS for Au and Pd, respectively, Figure 6). The difference in values is due to the use of the pseudo-reference C-PDMS and to the nature of the C-PDMS electrodes. The stripping processes take place at around 0.26 and 0.30 V/C-PDMS for Au and Pd respectively, with behaviors similar to those described on glassy carbon electrodes. At 1 µL min^{-1}, the voltammograms on both WE$_{DEP}$ and WE$_{det}$ for Au and Pd do not show a wave-shaped signal, except for Au on WE$_{det}$ (Figure 6-a). Indeed, the presence of a metal deposit on C-PDMS electrode such as Pd catalyzes hydroxonium ions reduction, leading to the overlapping of reduction signals and possibly to some interferences, as it will be discussed later.

Figure 6 – Cyclic voltammograms of (a) 500 µmol L^{-1} Au in 0.14 mol L^{-1} HCL and (b) 1000 µmol L^{-1} Pd in 0.1 mol L^{-1} HCl on WE$_{det}$ and WE$_{DEP}$ at 25 mV s^{-1} (static mode)

3.5. Au and Pd electrodeposition as a function of applied potential and flow rate

Experiments were performed by chronoamperometry within the microchannel under constant flow rate (1 µL min^{-1}) for different potentials. The deposition yields of both metals were evaluated separately. Three potential steps were successively applied at WE_{DEP} and at WE_{det}: *(i)* 0 V for 30 s to evaluate the current baseline, *(ii)* a constant potential between -0.4 and -1.2 V for 60 s to reduce metal ions and finally *(iii)* +0.5 V for more than 100 s to fully oxidize the metal deposits.

Figure 7 shows the chronoamperograms obtained at WE_{det} with the corresponding oxidation charges (third step) at both WE_{DEP} and WE_{det} as a function of the applied potential for metal reduction.

Figure 7 – (a) Chronoamperograms (i & ii) of 1000 µmol L^{-1} Pd in 0.1 mol L^{-1} HCl and 500 µmol L^{-1} Au in 0.14 mol L^{-1} HCL at WE_{det} under 1 µL min^{-1} flow rate with WE_{DEP} polarized at various potential and (b) oxidation charges corresponding to the third step measured at WE_{det} and on WE_{DEP} as a function of the reduction potential applied to WE_{DEP} during the second step.

The depletion yield as a function of flow rate for both metals is given in Figure 8. The same experiment than figure 7 was performed but without activation of WE_{DEP} so as to estimate the depletion yield, calculated from the oxidation charges Q developed at WE_{DEP} and WE_{det} during the third step as follows:

$$Depletion\ yield_{CA}\ (\%) = \left(1 - \frac{Q_{WEdet}\ with\ WE^{ON}_{DEP}}{Q_{WEdet}\ with\ WE^{ON}_{DEP}}\right) \times 100 \qquad \textbf{eq.5}$$

Note that the calculation of the depletion yield was not based on cathodic charges because the metal reductions are prone to interferences from solvent reduction. The highest depletion yields were obtained for the lowest flow rates, as previously observed for FcMeOH, namely 68.2 and 44.6 % for Au and Pd, respectively at 1 µL min^{-1}.

Figure 8 – Depletion yield estimated from Eq. 5 for Pd and Au as a function of the flow rate. (500 µmol L^{-1} Au in 0.14 mol L^{-1} HCl, 1 mmol L^{-1} Pd in 0.1 mol L^{-1} HCl, 200 µmol L^{-1} FcMeOH in phosphate buffer 0.2 mol L^{-1}, first step (0 to 30 s): WE_{det} = 0 V/C-PDMS; second step (30 to 90 s): WE_{det} = -1 V, -1.2 V and +1 V/C-PDMS for Au, Pd and FcMeOH, respectively, and third step (90 to 200 s): WE_{det} = 0.5 V/C-PDMS (for Pd and Au, only). WE_{DEP} is set at the same potential than WE_{det} when activated.

3.6. Depletion yield as a function of metal concentration and mechanism of deposition

The previously described results allowed setting the optimum parameters for the depletion of precious metals as follows: reduction potential values of -1.0 and -1.2 V for Au and Pd, respectively and minimal flow rate of 1 µL min^{-1}. The evaluation of the depletion yield as a function of the metal concentration in acidic solution was then performed (Figure 9) using the same procedure as in Figure 8 for concentrations ranging between 25 and 500 µmol L^{-1} for Au and for concentrations ranging between 25 to 1000 µmol L^{-1} for Pd.

Figure 9 – Depletion yield of Au and Pd as function of their concentration for flow rate of 1 µL min^{-1}. Same conditions as in Figure 8.

The data showed that the depletion yield decreased with the increase in concentration for both metals, with values of up to 89% for Pd (25 µmol L^{-1} / 2.7 mg L^{-1}) and 71 % for Au (25 µmol L^{-1} / 4.9 mg L^{-1}). These results are promising since they are obtained for concentrations close to the expected ones in real leach liquors from waste printed circuits boards recycling processes (9.4 to 94.0 mg L^{-1} for Pd and 5.1 to 50.8 mg L^{-1} for Au) [24].

Simulations performed under similar conditions predicted a depletion yield of 89% at 2.6 µL min^{-1}, which is higher than the experimental one. The difference between theoretical and experimental values can be attributed to several factors as discussed for FcMeOH, but other issues can also affect the process in the case of the metal deposition. Indeed, for Au the deposition of the metal occurs through its reduction into Au(+I) (as described by eq. 4) followed by the formation of Au(0) by dismutation. This phenomenon occurs after adsorption of gold complexes onto active sites, leading to the formation of multiple entities assimilated to nanoparticles [22]. The deposition of Au occurs in parallel to the formation of Au(+III), thus a fraction of the sample doesn't turn into solid and it is removed from the system without any treatment and being recovered. For Pd, the mechanism of growth of metallic deposit is discussed in the literature since it does not seem to correspond to a simple model where the ion is reduced on existing nuclei sites [25]. Depending on the applied potential, the growth of Pd can be described by different models [26] and only for high overpotential reduction value, bulk Pd deposit is observed [27]. In our case, the applied potential during the reduction step of chronoamperometric experiment corresponds to high overpotential, which is in favor of the formation of bulk metals. Moreover, since this potential value is high, reduction of the solvent overlaps the metal reduction and this leads to loss of performances of the electrode, explaining the impossibility to reach high depletion yield. The fact is that as soon as the deposition process begins for a given metal, the formation of the metal on the C/PDMS electrodes can induce a change in the reduction of metal complexes. This was evaluated by measuring the mean current of reduction of each metal on C-PDMS electrode previously modified with the same metal deposit. As illustrated in Figure 10, the mean current of metal ion reduction obtained by chronoamperometry on C-PDMS or on metal modified C-PDMS electrode are represented as a function of the applied potential (with blank subtraction).

Figure 10 – Mean current value obtained by chronoamperometry as a function of the potential for (a) 1000 µmol L^{-1} Pd in 0.1 mol L^{-1} HCl and (b) 500 µmol L^{-1} Au in 0.14 mol L^{-1} HCl at WE_{DEP} C-PDMS electrode (open square) and WE_{DEP} C-PDMS modified electrode (solid square). Metal deposits were performed at -1 V/C-PDMS on WE_{DEP} for 120s without flow. The same experiments with WE_{det} let to similar results (data not shown).

In the case of Au, the current related to the reduction of the metal complex is higher on Au-modified electrode than on C-PDMS for all the considered potential range. This can be attributed to a higher active surface or to a thermodynamically more favourable deposition on Au substrates. Thus, thin layered gold modification of C-PDMS electrode material is recommended to enhance the performances of the process. In the case of Pd, the current related to Pd reduction is clearly lower on Pd-modified electrode than on C-PDMS electrode for all the considered potential range. This can be explained by the fact that Pd acts as a catalyst at such a high reduction potential for the hydroxonium reduction. The reduction of Pd is thus overlapping with that of protons. This leads to a decrease of the deposition rate and potentially explains why the depletion yield cannot be larger. All these results demonstrate also why the depletion yield for Au is much higher than for Pd (Figure 8).

4. Conclusion

The depletion of precious metals on home-made reversibly bonded microchips was demonstrated with the integration of graphite/PDMS microelectrodes within microfluidic channels. It offers the unique advantage of allowing easy washing of the microchannel and renewal of the electrode surface by simply repositioning the microband electrodes which allows this type of device to have a relatively much longer lifespan than irreversibly closed ones. After characterization of process performances with a model electroactive probe (FcMeOH), this device was applied for the electrodeposition of Au and Pd, with a depletion yield of up to 89% for Pd and 71% for Au. These values were obtained for low metal concentration (25 µmol L^{-1}), which is in the range of those expected from leach liquors of PCBs wastes, undergoing a hydrometallurgical treatment. In order to further increase the depletion yield, other experimental parameters can be explored, such as the electrode size so as to increase the overall active surface and to overcome surface defaults. Such a microchip thus opens the way for real leach liquor treatment from the waste electric equipment recycling industry or for wastewater purification. To do so, a focus is therefore recommended on the optimization of the confinement on which this process is based, so as to increase the depletion yield. Indeed, this setup can be implemented on industrial scale provided that the confinement is ensured and optimized. It can also be used as a promising tool for the depletion of contaminant species whose removal rests on their electrochemical reactivity, such as organic pollutants or inorganic ions.

5. Acknowledgements

This work was supported by the French Environment and Energy Management Agency (ADEME) and the Chaire "Mines Urbaines" from ParisTech foundation, supported by Eco-systèmes. This work has received support of "Institut Pierre-Gilles de Gennes" (Laboratoire d'excellence: ANR-10-LABX-31, "Investissements d'avenir": ANR-10-IDEX-0001-02 PSL and Equipement d'excellence: ANR-10-EQPX-34).

6. Reference

[1] Rapport annuel du registre des Déchets d'Équipements Électriques et Électroni..., ADEME. (n.d.). http://www.ademe.fr/rapport-annuel-registre-dechets-dequipements-electriques-electroniques-deee-donnees-2015 (accessed August 22, 2017).

[2] V. Goodship, A. Stevels, J. Huisman, Waste Electrical and Electronic Equipment (WEEE) Handbook, Woodhead Publishing, 2019.

[3] B. Ghosh, M.K. Ghosh, P. Parhi, P.S. Mukherjee, B.K. Mishra, Waste Printed Circuit Boards recycling: an extensive assessment of current status, Journal of Cleaner Production. 94 (2015) 5–19. https://doi.org/10.1016/j.jclepro.2015.02.024.

[4] P.O. of the E. Union, Report on critical raw materials and the circular economy., (2018). https://publications.europa.eu/en/publication-detail/-/publication/d1be1b43-e18f-11e8-b690-01aa75ed71a1/language-en/format-PDF (accessed December 20, 2018).

[5] M. Kaya, Recovery of metals and nonmetals from electronic waste by physical and chemical recycling processes, Waste Management. 57 (2016) 64–90. https://doi.org/10.1016/j.wasman.2016.08.004.

[6] G.M. Whitesides, The origins and the future of microfluidics, Nature. 442 (2006) 368–373. https://doi.org/10.1038/nature05058.

[7] Les micro-réacteurs : opportunités et applications pour les industries chimiques - 2007, Direction Générale des Entreprises (DGE). (n.d.). https://www.entreprises.gouv.fr/secteurs-professionnels/micro-reacteurs-opportunites-et-applications-pour-industries-chimiques-2007 (accessed April 24, 2019).

[8] P.L. Suryawanshi, S.P. Gumfekar, B.A. Bhanvase, S.H. Sonawane, M.S. Pimplapure, A review on microreactors: Reactor fabrication, design, and cutting-edge applications, Chemical Engineering Science. 189 (2018) 431–448. https://doi.org/10.1016/j.ces.2018.03.026.

[9] D. M. Roberge, M. Gottsponer, M. Eyholzer, N. Kockmann, Industrial design, scale-up, and use of microreactors, Chimica Oggi. 27 (2009) 8–11.

[10] M. Yew, Y. Ren, K.S. Koh, C. Sun, C. Snape, A Review of State-of-the-Art Microfluidic Technologies for Environmental Applications: Detection and Remediation, Glob. Chall. 3 (2019) 1800060. https://doi.org/10.1002/gch2.201800060.

[11] C. Tian, Q. Tu, W. Liu, J. Wang, Recent advances in microfluidic technologies for organ-on-a-chip, Trac-Trends Anal. Chem. 117 (2019) 146–156. https://doi.org/10.1016/j.trac.2019.06.005.

[12] T. Watanabe, S. Shibano, H. Maeda, A. Sugitani, M. Katayama, Y. Matsumoto, Y. Einaga, Fabrication of a Microfluidic Device with Boron-doped Diamond Electrodes for Electrochemical Analysis, Electrochimica Acta. 197 (2016) 159–166. https://doi.org/10.1016/j.electacta.2015.11.035.

[13] R. Oliveira, C. Sella, C. Souprayen, E. Ait-Yahiatene, C. Slim, S. Griveau, L. Thouin, F. Bedioui, Development of a flow microsensor for selective detection of nitric oxide in the presence of hydrogen peroxide, Electrochimica Acta. 286 (2018) 365–373. https://doi.org/10.1016/j.electacta.2018.07.158.

[14] C. Amatore, N. Da Mota, C. Sella, L. Thouin, Theory and Experiments of Transport at Channel Microband Electrodes under Laminar Flows. 1. Steady-State Regimes at a Single Electrode, Anal. Chem. 79 (2007) 8502–8510. https://doi.org/10.1021/ac070971y.

[15] C. Amatore, N. Da Mota, C. Lemmer, C. Pebay, C. Sella, L. Thouin, Theory and Experiments of Transport at Channel Microband Electrodes under Laminar Flows. 2. Electrochemical Regimes at Double Microband Assemblies under Steady State, Anal. Chem. 80 (2008) 9483–9490. https://doi.org/10.1021/ac801605v.

[16] R. Oliveira, F. Bento, C. Sella, L. Thouin, C. Amatore, Direct Electroanalytical Method for Alternative Assessment of Global Antioxidant Capacity Using Microchannel Electrodes, Anal. Chem. 85 (2013) 9057–9063. https://doi.org/10.1021/ac401566w.

[17] K. Anwar, T. Han, S.M. Kim, Reversible sealing techniques for microdevice applications, Sensors and Actuators B: Chemical. 153 (2011) 301–311. https://doi.org/10.1016/j.snb.2010.11.002.

[18] R.S. Martin, A.J. Gawron, S.M. Lunte, C.S. Henry, Dual-Electrode Electrochemical Detection for Poly(dimethylsiloxane)-Fabricated Capillary Electrophoresis Microchips, Anal. Chem. 72 (2000) 3196–3202. https://doi.org/10.1021/ac000160t.

[19] J.M. Petroni, B.G. Lucca, V.S. Ferreira, Simple approach for the fabrication of screen-printed carbon-based electrode for amperometric detection on microchip electrophoresis, Analytica Chimica Acta. 954 (2017) 88–96. https://doi.org/10.1016/j.aca.2016.12.027.

[20] J. Gouyon, F. d'Orlyé, S. Griveau, F. Bedioui, A. Varenne, Characterization of home-made graphite/PDMS microband electrodes for amperometric detection in an original reusable glass-NOA®-PDMS electrophoretic microdevice, Electrochimica Acta. 329 (2020) 135164. https://doi.org/10.1016/j.electacta.2019.135164.

[21] C. Cannes, F. Kanoufi, A. J Bard, Cyclic voltammetry and scanning electrochemical microscopy of ferrocenemethanol at monolayer and bilayer-modified gold electrodes, Journal of Electroanalytical Chemistry. 547 (2003) 83–91. https://doi.org/10.1016/S0022-0728(03)00192-X.

[22] L. Komsiyska, G. Staikov, Electrocrystallization of Au nanoparticles on glassy carbon from HClO 4 solution containing [AuCl 4] −, Electrochimica Acta. 54 (2008) 168–172. https://doi.org/10.1016/j.electacta.2008.08.013.

[23] G. Chang, Y. Luo, W. Lu, X. Qin, A.M. Asiri, A.O. Al-Youbi, X. Sun, Electrodeposition Fabrication of Pd Nanoparticles on Glassy Carbon Electrode Towards Methanol Oxidation Application, Current Research in Nanotechnology. 4 (2013) 1–7. https://doi.org/10.3844/ajnsp.2013.1.7.

[24] E. Kim, M. Kim, J. Lee, B.D. Pandey, Selective recovery of gold from waste mobile phone PCBs by hydrometallurgical process, Journal of Hazardous Materials. 198 (2011) 206–215. https://doi.org/10.1016/j.jhazmat.2011.10.034.

[25] S. Gu, X. Wang, Y. Wei, B. Fang, Mechanism for nucleation and growth of electrochemical deposition of palladium(II) on a platinum electrode in hydrochloric acid solution, Sci. China Chem. 57 (2014) 755–762. https://doi.org/10.1007/s11426-013-5026-2.

[26] A. Alvarez, D.R. Salinas, Formation of Cu/Pd bimetallic crystals by electrochemical deposition, Electrochimica Acta - ELECTROCHIM ACTA. 55 (2010) 3714–3720. https://doi.org/10.1016/j.electacta.2010.01.076.

[27] A. Sahin, Q. Huang, J.M. Cotte, B.C. Baker-O'Neal, Electrochemical Palladium Deposition for Reducing Critical Dimensions in Nanostructures, J. Electrochem. Soc. 161 (2014) D697–D703. https://doi.org/10.1149/2.0851412jes.

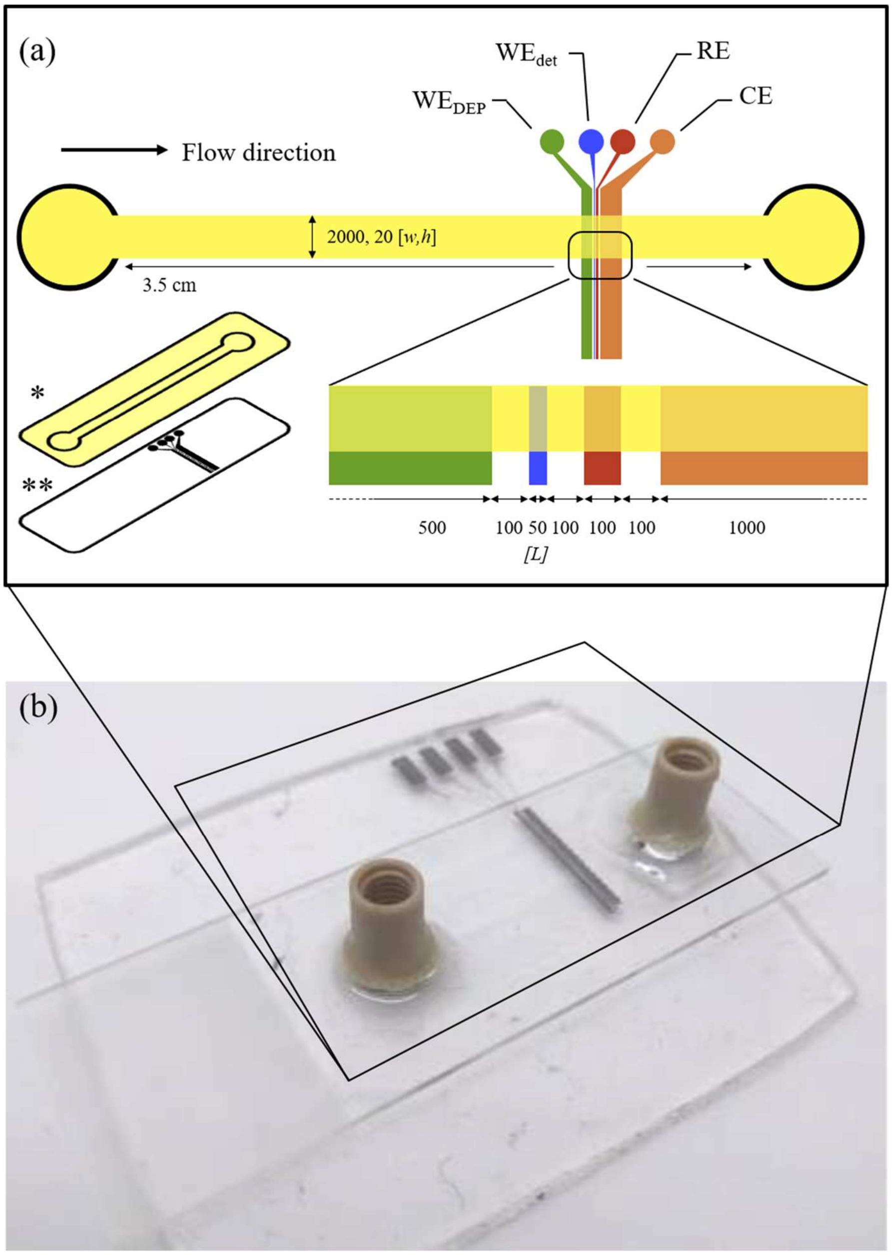

Figure 1 – (a) Scheme of microchannel with four integrated C/PDMS microbands electrodes. WEDEP is dedicated to the depletion process (and thus to the recovery), WEdet is dedicated to the determination of the considered species and thus to the evaluation of the recovery efficiency. Dimensions in µm (unless specified). * upper part of the setup (NOA81® microchannel; ** lower part of the setup (C-PDMS electrodes in PDMS substrate) (b) Photography of the experimental setup

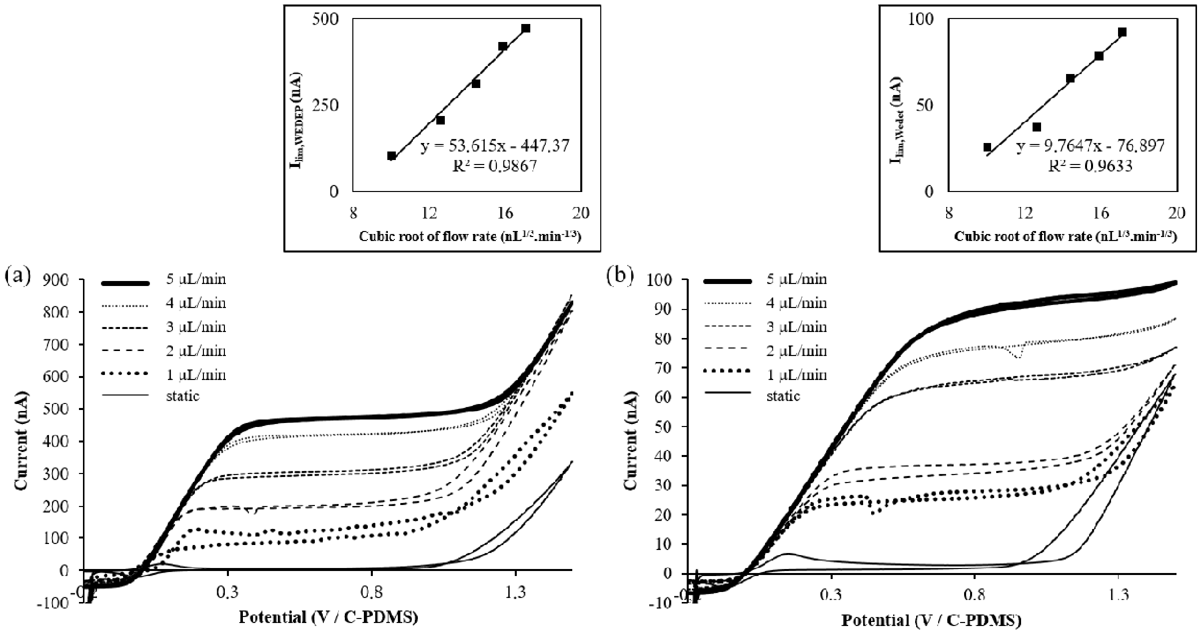

Figure 2 – Cyclic voltammograms of 200 µmol.L^{-1} FcMeOH in 0.2 mol.L^{-1} phosphate buffer at (a) WE$_{DEP}$ and (b) WE$_{det}$, in static mode (full line) and under continuous flow (from 1 to 5 µL.min^{-1}). Scan rate: 25 mV.s^{-1}. Inserts correspond to the plots of limiting currents as a function of cubic root of flow rate.

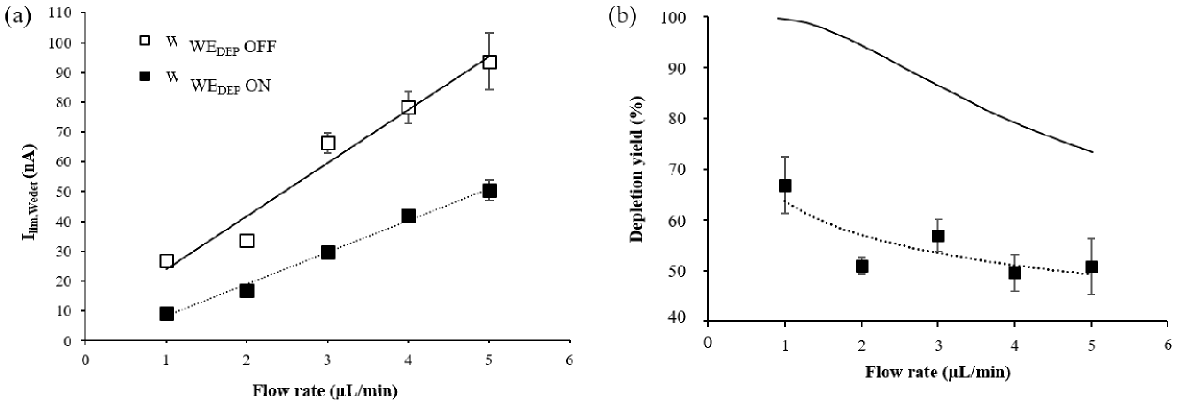

Figure 3 – (a) Limiting currents measured by cyclic voltammetry (from data in Fig. 2) at $\mathrm{WE_{det}}$ without (OFF) and with (ON) polarization of $\mathrm{WE_{DEP}}$. (b) Corresponding depletion yield evaluated from eq.1 as a function of flow rate. $\mathrm{WE_{DEP}}$ is biased at 1.0 V when polarized (ON).

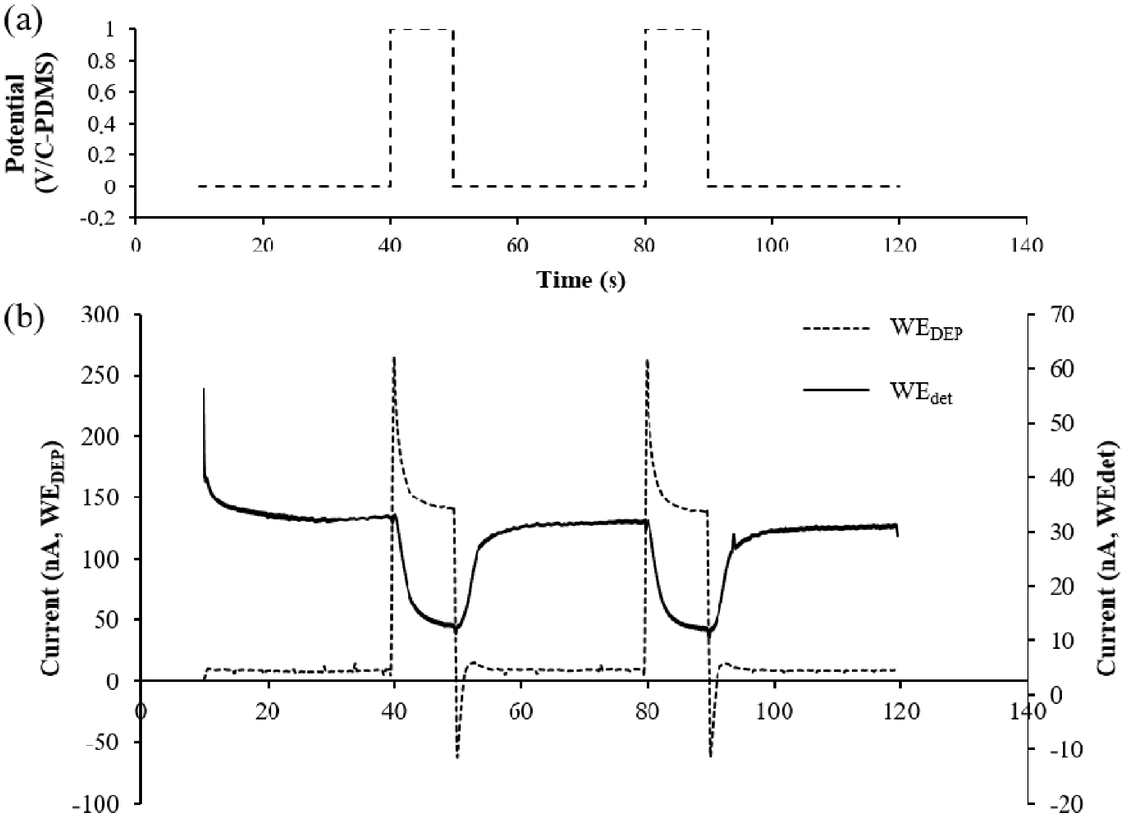

Figure 4 – (a) Potential steps applied to WE$_{DEP}$ for successive activations (1 V) and deactivations (0 V) of the depletion process. WE$_{det}$ is continuously polarized at 1 V. (b) Corresponding chronoamperograms monitored at WE$_{det}$ (full line) and WE$_{DEP}$ (dashed line). 200 µmol.L^{-1} FcMeOH in 0.2 mol.L^{-1} phosphate buffer and flow rate of 1 µL.min^{-1}.

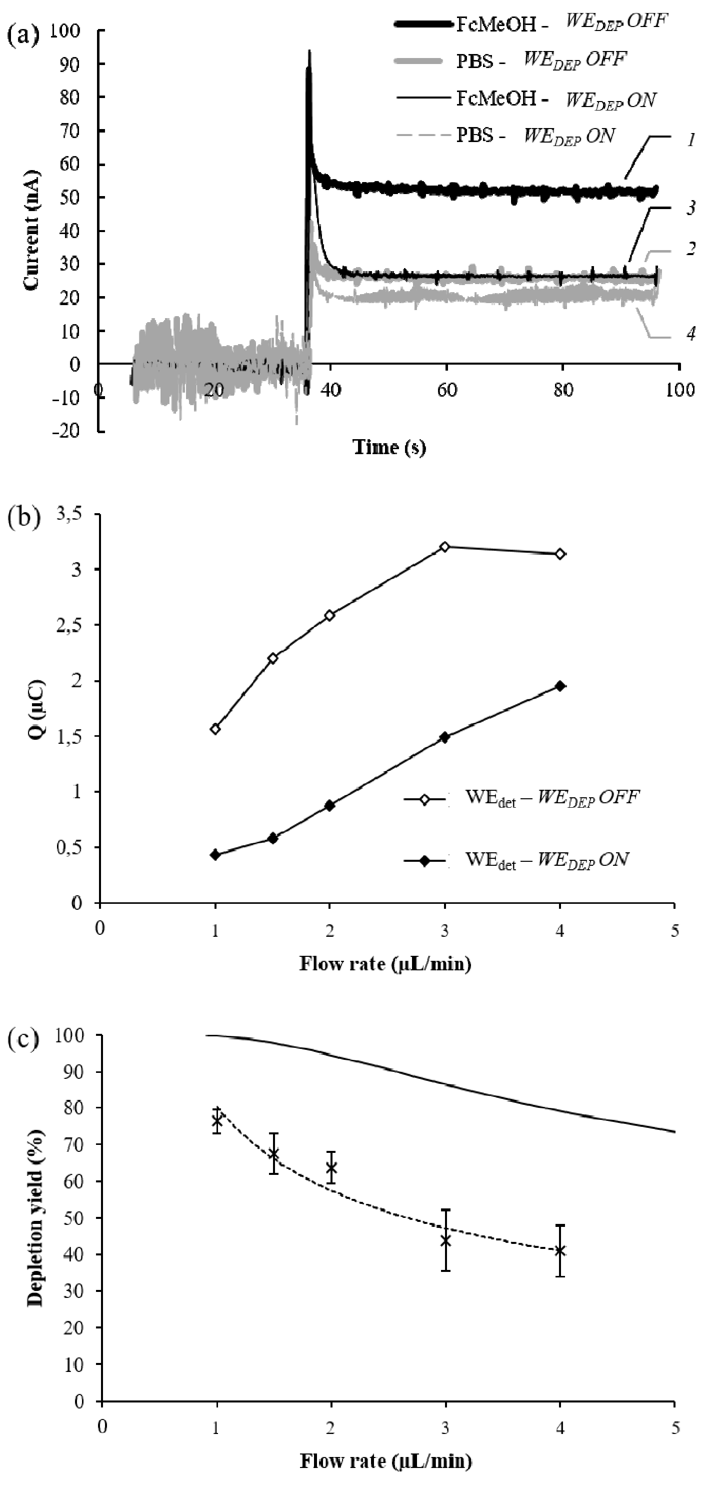

Figure 5 – (a) Chronoamperometry at WE_{det} (30 s at 0 V and 60 s at 1.0 V) without depletion (curves 1 and 2, WE_{DEP} OFF) and with depletion (curves 3 and 4, WE_{DEP} polarized at 1 V) at 1 µL.min^{-1} flow rate. (b) Experimental charge Q_{WEdet} developed at WE_{det} during the second step as a function of flow rate. (c) Depletion yield evaluated by eq. 2 from experimental data (cross points, dashed line) and simulations (solid curve) as a function of flow rate (200 µmol.L^{-1} FcMeOH in 0.2 mol.L^{-1} phosphate buffer).

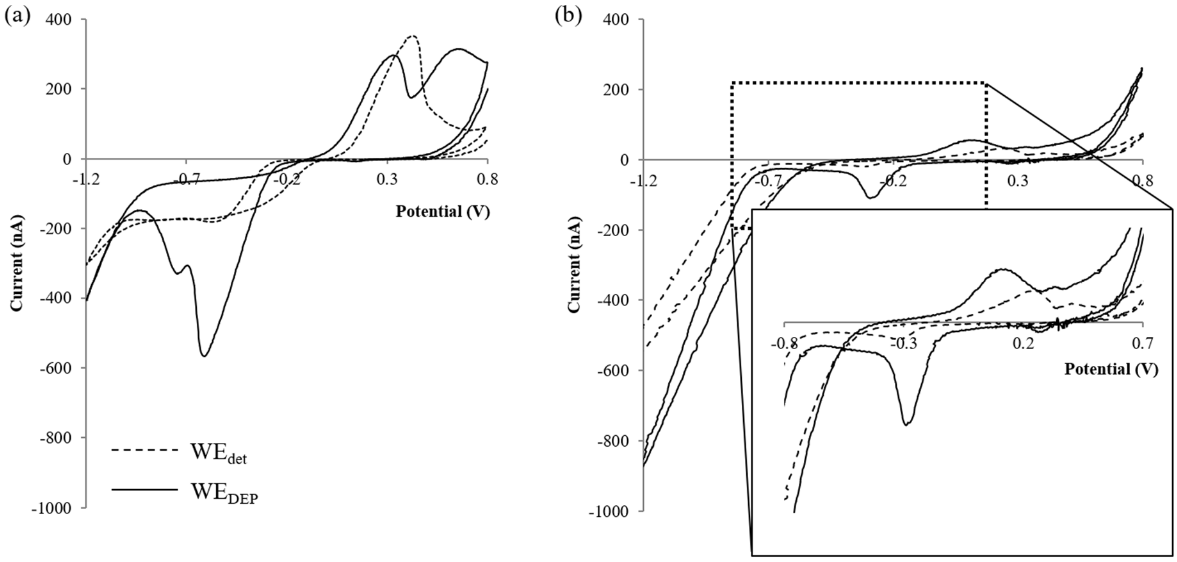

Figure 6 – Cyclic voltammograms of (a) 500 μmol.L^{-1} Au in 0.14 mol.L^{-1} HCL and (b) 1000 μmol.L^{-1} Pd in 0.1 mol.L^{-1} HCl on WE$_{det}$ and WE$_{DEP}$ at 25 mV/s (static mode)

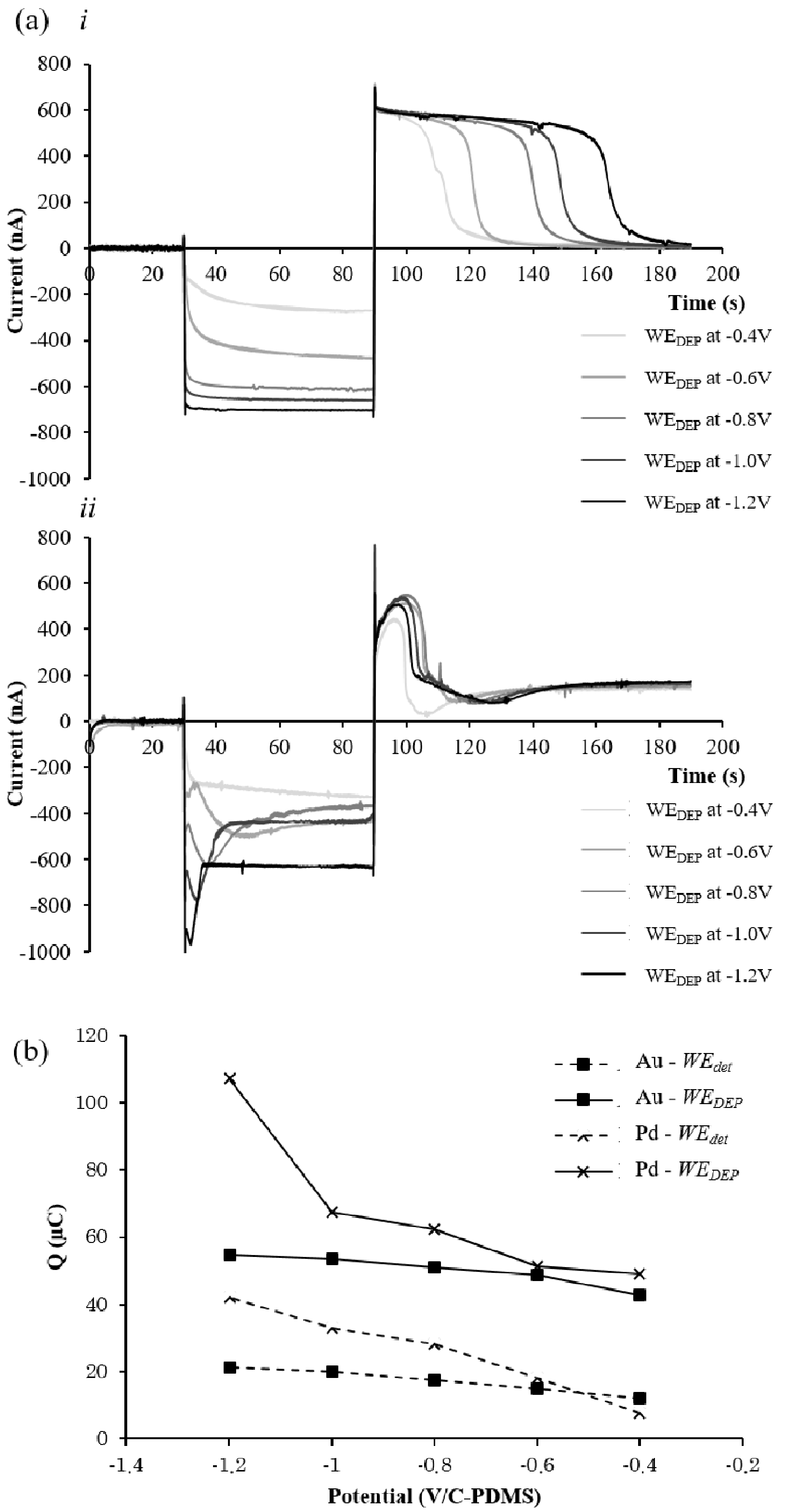

Figure 7 – (a) Chronoamperograms (i & ii) of 1000 μmol.L^{-1} Pd in 0.1 mol.L^{-1} HCl and 500 μmol.L^{-1} Au in 0.14 mol.L^{-1} HCL at WE$_{det}$ under 1 μL.min^{-1} flow rate with WE$_{DEP}$ polarized at various potential and (b) oxidation charges corresponding to the third step measured at WE$_{det}$ and on WE$_{DEP}$ as a function of the reduction potential applied to WE$_{DEP}$ during the second step.

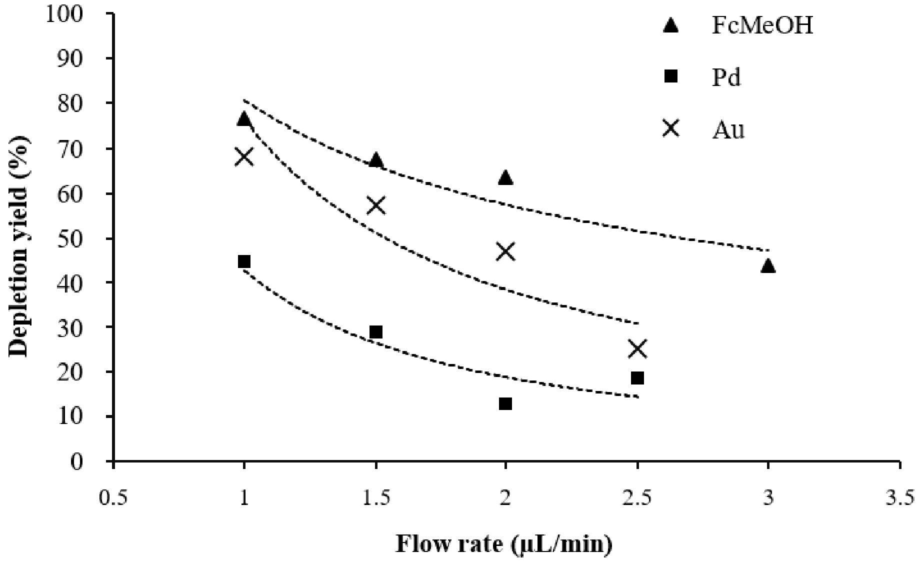

Figure 8 – Depletion yield estimated from Eq. 5 for Pd and Au as a function of the flow rate. (500 µmol.L^{-1} Au in 0.14 mol.L^{-1} HCl, 1 mmol.L^{-1} Pd in 0.1 mol.L^{-1} HCl, 200 µmol.L^{-1} FcMeOH in phosphate buffer 0.2 mol.L^{-1}, fist step (0 to 30 s): WE$_{det}$ = 0 V/C-PDMS; second step (30 to 90 s): WE$_{det}$ = -1 V, -1.2 V and +1 V/C-PDMS for Au, Pd and FcMeOH, respectively, and third step (90 to 200 s): WE$_{det}$ = 0.5 V/C-PDMS (for Pd and Au, only). WE$_{DEP}$ is set at the same potential than WE$_{det}$ when activated.

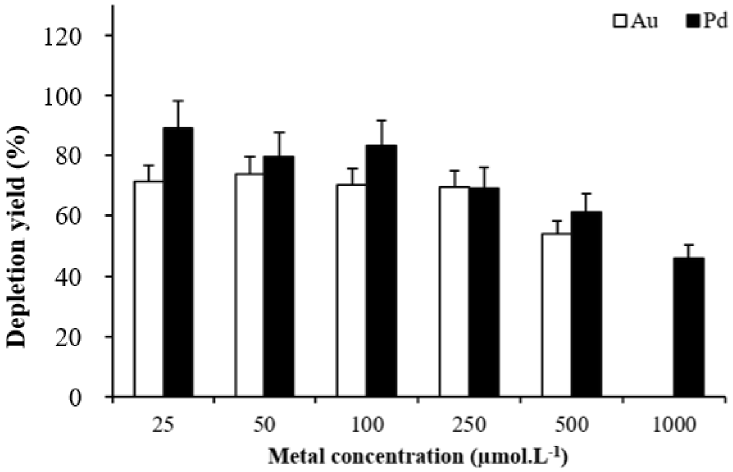

Figure 9 – Depletion yield of Au and Pd as function of their concentration for flow rate of 1 µL.min^{-1} . Same conditions as in Figure 8.

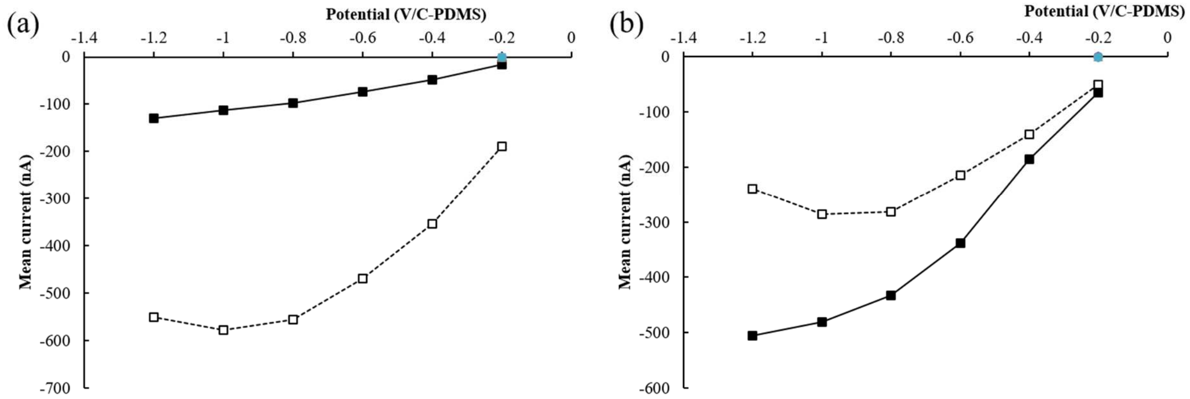

Figure 10 – Mean current value obtained by chronoamperometry as a function of the potential for (a) 1000 µmol.L^{-1} Pd in 0.1 mol.L^{-1} HCl and (b) 500 µmol.L^{-1} Au in 0.14 mol.L^{-1} HCl at WE$_{DEP}$ C-PDMS electrode (open square) and WE$_{DEP}$ C-PDMS modified electrode (solid square). Metal deposits were performed at -1 v:C-PDMS on WE$_{DEP}$ for 120s without flow. The same experiments with WE$_{det}$ let to similar results (data not shown).